Propagating-arc magnetohydrodynamic plasma actuator for directional high-authority flow control in atmospheric air



2013 J. Phys. D: Appl. Phys. 46 485208

(http://iopscience.iop.org/0022-3727/46/48/485208)

IOP Publishing Journal of Physics D: Applied Physics
J. Phys. D: Appl. Phys. **46** (2013) 485208 (7pp) doi:10.1088/0022-3727/46/48/485208

# Propagating-arc magnetohydrodynamic plasma actuator for directional high-authority flow control in atmospheric air

**Brent Pafford, Jayant Sirohi and Laxminarayan L Raja**[1]

Department of Aerospace Engineering and Engineering Mechanics, The University of Texas at Austin, Austin, TX 78712, USA

E-mail: jayant.sirohi@mail.utexas.edu and lraja@mail.utexas.edu

Received 11 May 2013, in final form 30 August 2013
Published 12 November 2013
Online at stacks.iop.org/JPhysD/46/485208

**Abstract**
A propagating-arc magnetohydrodynamic plasma actuator for aerodynamic flow control is reported. The actuator comprises two rail electrodes flush mounted on an aerodynamic surface. A pulsed arc is propelled down the length of the rails by Lorentz forces supported by a self-induced magnetic field. The arc induces a high velocity pulsed air wall jet due to the pushing and entrainment actions. Experiments in quiescent air demonstrate that the plasma arc achieves a peak velocity of around 100 m s$^{-1}$ and requires a discharge energy on the order of 300 J per pulse. Wind tunnel tests on a 14.5 inch chord airfoil section, at a Reynolds number of 0.45 million show induced flow velocities on the order of 10's m s$^{-1}$ with significant penetration of the flow actuation effect perpendicular to the wall surface.

(Some figures may appear in colour only in the online journal)

## 1. Introduction

Plasma actuators are attractive for aerodynamic flow control applications due to the absence of moving parts, extremely fast response times, and conformability to aerodynamic surfaces. There has been considerable recent research on plasma actuators that operate at atmospheric pressure conditions with minimal structural modification to the aerodynamic surface while inducing highly directional flow velocities [1]. In particular, non-equilibrium surface dielectric barrier discharges (DBD) have witnessed significant interest because of their geometric simplicity, low power consumption and wide area coverage over the aerodynamic surface [2–6]. Flow actuation by DBDs is supported by the ionic wind phenomenon that is active when electrostatic fields act on net space-charge regions of the discharge [7]. Highly directional electrohydrodynamic forcing of the flow can be realized, however this mechanism has inherent limitations. The size of the net space-charge region, where the electrohydrodynamic forcing is active, scales with the plasma Debye length which decreases with increasing plasma density, thereby resulting in an upper bound on the achievable induced flow velocity. A similar upper limit on the velocity results from charge deposition on the dielectric surface that causes a secondary breakdown and has a negative influence on the DBD actuator performance [8]. As a result, over a decade of research on DBDs and related plasma flow actuators has not yielded induced flow velocities in excess of a few m s$^{-1}$. This limitation is manifest in the relatively low Mach numbers and Reynolds numbers ($<10^6$) at which most of the successful applications of DBDs have been reported [1, 4, 6, 9].

Actuation of atmospheric aerodynamic flows can also be achieved through gas dilatational effects from localized heating of the air by arc filament plasmas, but this mechanism is non-directional [10, 11]. Variants of the above that use arc filaments embedded within surface cavities can achieve directional flow actuation through arc heating induced jet action, but such approaches are generally undesirable because of concerns with localized hot spots on the modified surfaces [12].

[1] Author to whom any correspondence should be addressed.

 

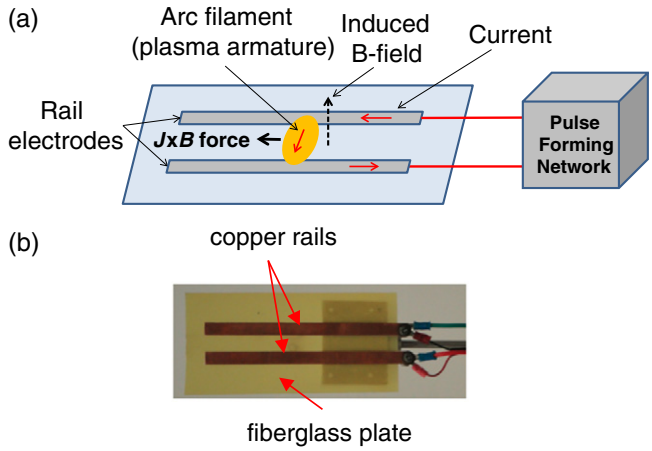


**Figure 1.** (*a*) Schematic illustration of the rail plasma actuator (RailPAc) concept and (*b*) top-down picture of prototype bench-scale RailPAc with 150 mm long copper rails.

## 2. The rail plasma actuator concept

Here, we describe a magnetohydrodynamic (MHD) approach to aerodynamic flow actuation at atmospheric pressure. The concept is illustrated in figure 1(*a*) and involves a pair of parallel conducting strip electrodes (called 'rails') that are flush mounted on a dielectric aerodynamic surface. A pulse forming network is connected to the rails, and initiates a localized arc discharge at one end. The arc can be sustained by a relatively low voltage (∼100 V) and large current (∼1 kA) for a short duration of time (typically ∼ few ms) depending on the characteristics of the pulse forming network. The current ($J$) passing through the rails and the plasma arc induces a magnetic field ($B$), which in turn generates a strong Lorentz force ($J \times B$) on the plasma arc column, accelerating it along the rails away from the network connection point (figure 1(*a*)). At high (atmospheric) pressures, the arc is relatively impermeable and its motion readily couples momentum into the surrounding air [13, 14]. A moving arc column therefore results in compression of air ahead of the arc and entrainment of air behind the arc. These processes combine to induce aerodynamic flow in the form of a pulsed wall jet. The induced flow velocity is therefore coupled to the velocity of the arc motion. The device is termed the rail plasma actuator (RailPAc). The principle of RailPAc operation is similar to the magnetically driven surface discharge actuator reported by Kalra *et al* [15]. However, their device required a large (∼5 T) external magnetic field supplied by a solenoid, and operated at low sub-atmospheric pressures (∼30 Torr) and low arc currents (∼100 mA).

The velocity of the plasma arc depends on a balance between the Lorentz force and the aerodynamic drag acting on it. The voltage applied by the pulse forming network and the resulting arc current can therefore be used to directly control the arc velocity. Furthermore, the device can be repetitively pulsed to create a quasi-continuous induced wall jet. An important consequence of the rail electrode configuration is that the length of rail electrode pair must be oriented along the desired flow forcing direction. The region of flow forcing in the spanwise direction (direction perpendicular to the rail length) is therefore limited by the inter-electrode spacing. In contrast, in the DBD actuators, the electrodes are oriented perpendicular to the direction of flow forcing. A large spanwise portion of the flow determined by the electrode length can therefore be actuated by the DBD. For the rail plasma actuator to actuate a large spanwise portion of the flow, a multitude of rail electrode pairs placed parallel to each other can be used.

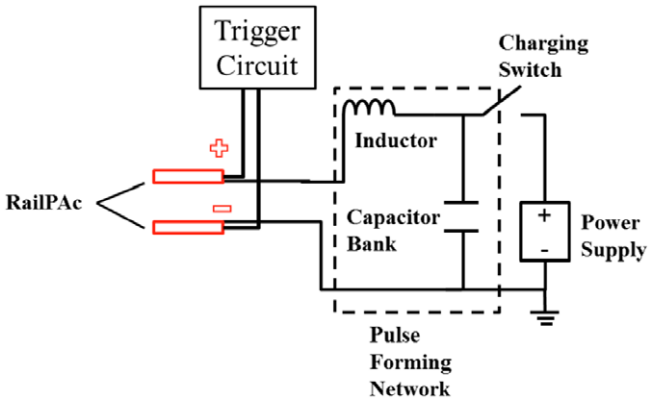


**Figure 2.** Pulse forming network with trigger circuit for arc initiation.

## 3. Experimental approach

We performed experiments on a bench-scale RailPAc device in quiescent atmospheric air. These experiments consisted of high-speed imaging of arc motion as well as electrical characterization of the device. We also embedded a prototype RailPAc in a two-dimensional airfoil and used a laser Doppler anemometer (LDA) to measure the induced velocity in the presence of an incident airstream. The plasma arc was initiated and sustained by a pulse forming network with the ability to repetitively create discharges at a desired rate.

### *3.1. Proof-of-concept prototype*

We constructed a proof-of-concept bench-scale prototype to qualitatively evaluate the operation of the RailPAc. A top-down picture of the device is shown in figure 1(*b*). The device comprises two parallel copper strips each measuring 150 mm long, 10 mm wide and 1.6 mm thick, separated by a distance of about 10 mm and bonded to a fiberglass plate. The right ends of the rails are connected to a pulse forming network that was designed and constructed in-house. This end forms the initiation region (breech) of the arc, which then transits the rails towards the left end (muzzle).

### *3.2. Pulse forming network*

The pulse forming network consists of a capacitor bank (six parallel Sprague Powerlytic 36DX electrolytic) with a total capacitance of 21 mF connected across the rails through a 15 $\mu$H air-core inductor (figure 2). The capacitor bank stores the energy that is dissipated during the plasma discharge, and the duration of the discharge is determined by the inductor. The capacitor bank is charged by a Xantrex XHR 600–1.7

direct current (dc) power supply through a charging switch. A high voltage (∼30 kV) is momentarily applied across the rails by a trigger circuit. This initiates a localized corona-like discharge at a specific point on the rails where the air gap is slightly reduced by a small protrusion. The corona discharge crosses the gap between the rails, creating a conductive path that quickly transitions into the arc. The time constant of the trigger circuit, set by a capacitor–resistor combination, can be tailored to a desired repetition rate targeting a specific unsteady flow phenomenon. Due to the continuous motion of the arc along the rails and the short transit time, there are no adverse thermal effects on the underlying structure from the plasma discharges. The capacitors were charged initially to different voltages ($V_c$), up to a maximum of 250 V. The time constant of the inductor–capacitor (LC) circuit was equal to 9.7 ms, which was experimentally found to be long enough for the arc to completely transit the length of the 150 mm rails.

### *3.3. Plasma arc velocity measurements*

A Vision Research high-speed digital camera was used to capture video of the arc motion. The digital images were used to measure the velocity of the plasma arc and the spatial extent of the arc. Top-down digital images of the arc were acquired at a rate of 76 000 frames per second with a window size of 256 × 64 pixels. Frontal view images were acquired at a rate of 47 000 frames per second with a window size of 512×256 pixels. To increase the precision of the measurement, the minimum camera aperture was selected (f-stop of 24), and a 10 mil. Mylar film lens was placed on the outside of the lens to act as a neutral-density filter and eliminate the bright superheated air that surrounds the plasma arc. The position of the nominal centre of the arc was tracked between frames of the high-speed video and this information was used to determine the velocity of the arc as a function of time.

### *3.4. Electrical measurements*

All electrical signals were acquired using a Tektronix 4 channel oscilloscope. The instantaneous current was measured using a Powertek–Rogowski current waveform transducer, secured around the positive electrical lead between the pulse forming network and the positive rail. This transducer measures the rate at which the charge flows through the transducer coil with respect to time; integration of this signal yields the instantaneous rail current. The voltage was measured using a differential voltage probe (Tektronix P5100A) coupled to the breech of the rails with the electrical leads.

### *3.5. Wind tunnel test article*

To evaluate the velocity profile induced by the RailPAc over an aerodynamic surface, a two-dimensional wind tunnel test article was fabricated with a S5010 airfoil with a span of 32.25 inch and a chord of 14.5 inch (figure 3). A RailPAc comprising two identical copper rail electrodes that are 10 mm wide and 300 mm long is embedded conformally on the upper surface of the airfoil along the chordwise direction, starting at 10% chord. The plasma arc is initiated at the leading edge

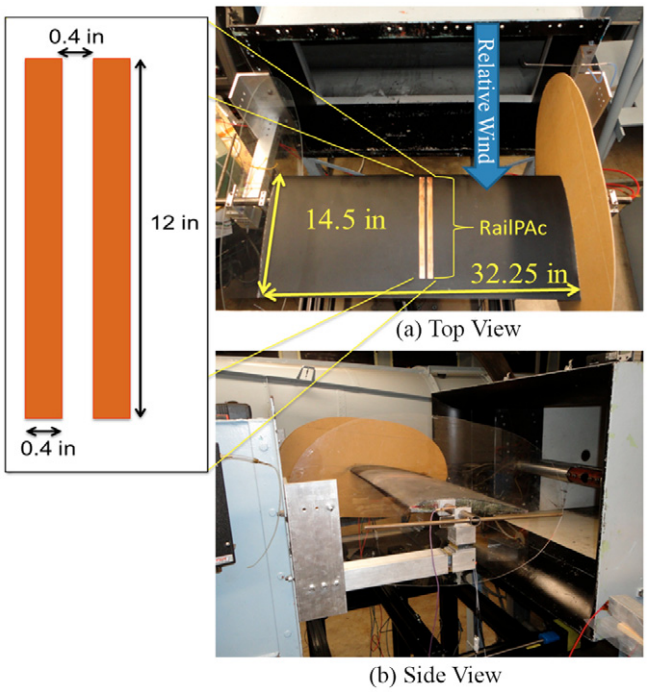


**Figure 3.** Wind tunnel test article consisting of RailPAc embedded in a 2D airfoil section.

of the rails and travels towards the trailing edge along the chordwise direction. Note that the copper rails conform to the airfoil profile without altering the shape or structural integrity and have a negligible weight penalty. When the actuators are not in use, the characteristics of the unaltered airfoil are retained. Therefore, the addition of the RailPAc electrodes has no adverse effects on the aerodynamic performance of the passive airfoil.

### *3.6. Induced flow measurements*

The wind tunnel test article was mounted in a subsonic, open test section, closed-circuit wind tunnel and secured by two supports external to the test section (figure 3(*b*)). A Dantec Dynamics LDA was used to capture pointwise measurements of the flow velocity immediately above the RailPAc at multiple free stream velocities, over a grid of points. The LDA transmitting and receiving optics were mounted below the test article on a graduated mechanical traverse, capable of moving the sensing head in the chordwise ($x$), spanwise ($z$) and normal ($y$) directions. For ease of access, the test article was placed upside down in the wind tunnel test section (figure 4) at a zero degree angle of attack. The wind tunnel freestream velocity was set as 16 m s$^{-1}$, which gives a chord based Reynolds number of approximately 0.45 million.

The measurement points of the LDA were located along a vertical line perpendicular to the airfoil surface about 225 mm from the leading edge of the airfoil (60% chord). Measurements were performed at a spacing of 3.25 mm and cover a vertical distance of 45 mm from the surface. A Rosco fog machine was used to create a dense water-based aerosol with mean seed particle size on the order of 1 $\mu$m. Based on this dimension and the free stream velocity, the Stokes number [16]

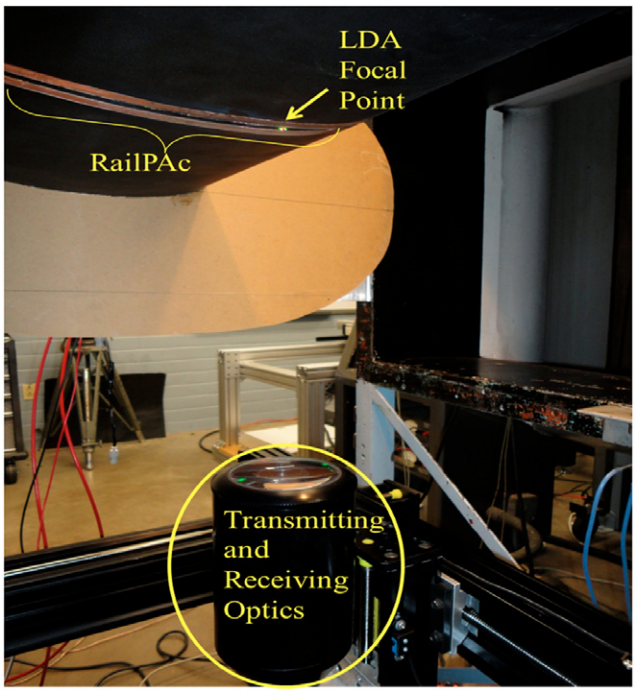


**Figure 4.** Experimental setup for measurement of velocity profile using the LDA.

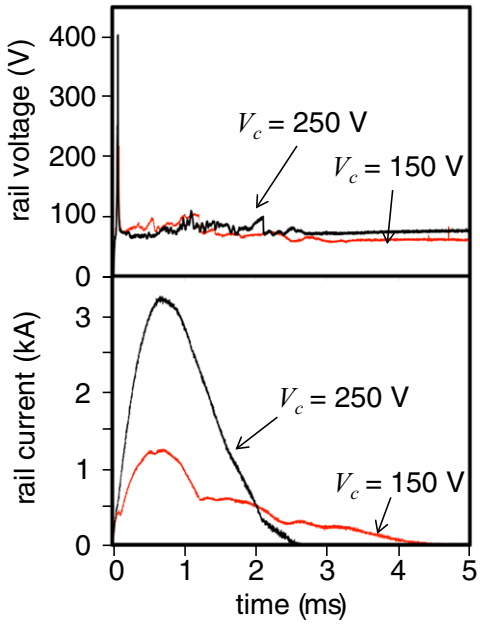


**Figure 5.** Rail voltage and current as a function of time and capacitor initial charge voltage.

of the seed particles was calculated to be on the order of $10^{-6}$, which results in an expected tracking error of less than 1% even in the presence of an induced wall jet of velocity on the order of 100 m s$^{-1}$.

The LDA measures the velocity of every seed particle that transitions through the measurement volume (less than a 1 mm$^3$) at each grid point. Over a 25 s sampling window, the LDA records the time of arrival as well as the transition time of the seed particle through the 1 mm beam width at the focal point. The individual velocities of seed particles flowing over the passive airfoil (RailPAc turned off) are used to calculate the mean velocity ($U_{\text{mean}}$) of the incident airstream. After the passive signal is stored, the test is repeated at the same location with the RailPAc discharging 10 plasma arcs at a frequency of 1.25 Hertz (Hz) during the 25 s sampling window. The velocity signal with RailPAc on is compared to the passive signal by calculating the average of multiple velocity peaks produced by the RailPAc.

Note that the open test section of the wind tunnel allows a large portion of the seed particles to escape, reducing the fog density. Because the LDA operates on the random arrival time of the seed particles, the sampling rate is random and at times very slow compared to the pulse duration of the arc (~2 ms). As a result, not all of the plasma arc transits are captured and recorded. Therefore, to properly analyse the results, the LDA processor is linked to the pulse forming network through a common reference trigger that is used to identify the transient velocity induced by the RailPAc.

## 4. Results and discussion

The transient voltage across the rails and the current through the rails for initial capacitor charge voltages of 150 V and 250 V are shown in figure 5. The voltages across the rails are characterized by initial spikes during the first 100 $\mu$s of the transient followed by relatively constant values for the remainder of the transient. The peak values of the rail voltage at the initial spikes are 216 V for $V_c$ = 150 V and 400 V for $V_c$ = 250 V. The initial spikes are higher than the capacitor voltages due to the transient voltage rise across the series inductor. The post-spike constant part of rail voltage transients show significant fluctuations until about 3 ms into the transient following which the voltage remains at steady values of about 70 V and 80 V for the $V_c$ = 150 V and $V_c$ = 250 V cases, respectively. The current transient shows a rapid increase until peak values (1.2 kA for $V_c$ = 150 V and 3.2 kA for $V_c$ = 250 V) are reached at about 0.8 ms, for both cases. Following this peak, the current drops until it reaches zero. The zero currents are reached about 4.2 ms and 2.4 ms into the transient for the $V_c$ = 150 V and $V_c$ = 250 V cases, respectively. The higher overall currents for the $V_c$ = 250 V are indicative of a lower arc resistance. At the time of peak current, the arc resistance is calculated from the rail voltage to be about 0.066 Ω for $V_c$ = 150 V and 0.025 Ω for $V_c$ = 250 V. The total energy dissipated in the discharge is readily calculated by a time integration of the product of the rail voltage and the current. A total of 114 J and 312 J are dissipated in the arc for the $V_c$ = 150 V and $V_c$ = 250 V cases, respectively. The initial energies stored in the capacitors ($E_{\text{cap}} = 1/2CV_c^2$) are 236 J and 656 J for the $V_c$ = 150 V and $V_c$ = 250 V cases, respectively. The capacitor voltages at the end of the transient are 70 V and 80 V, for the $V_c$ = 150 V and $V_c$ = 250 V cases resulting in a leftover energy of 51 J and 67 J respectively for the two cases. About 30% and 43% of the initial capacitor energy is therefore lost to non-discharge related parasitic processes in the system for the $V_c$ = 150 V and $V_c$ = 250 V cases. These parasitic processes include series resistance losses in the capacitor bank, the inductor coils and

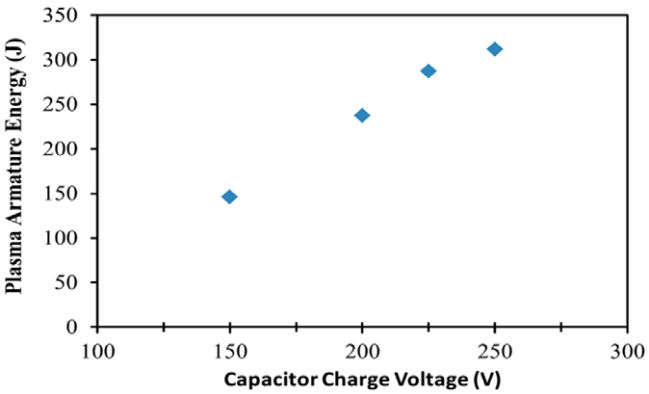


**Figure 6.** Arc energy as a function of initial capacitor charge voltage.

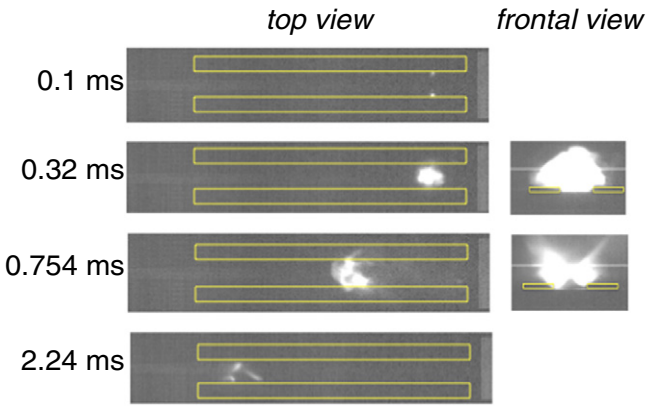


**Figure 7.** High-speed imaging of the RailPAc discharge for an initial capacitor voltage of 250 V. Top view images of the arc motion at 0.1, 0.32, 0.754 and 2.24 ms after the discharge initiation are shown. A frontal view of the arc is shown at 0.32 and 0.754 ms to illustrate the vertical extent of the arc from the surface. (Yellow rectangles indicate outline of rails. Gap between rails is 15 mm).

circuit connections. Figure 6 shows the relationship between capacitor charge voltage and energy consumed by the arc per pulse. The rate of increase of arc energy with voltage is seen to decrease at higher charge voltages.

Figure 7 shows four snapshots of the $V_c = 250$ V case in a top-down view at 0.1, 0.32, 0.754 and 2.24 ms after initiation. A frontal view looking into the length of the rails as the arc travels towards the camera is shown for 0.32 and 0.754 ms. It can be seen from the top-down view that the arc transits the rails from right to left and maintains a cohesive structure until about 2.24 ms after initiation, when it begins to extinguish. The arc is most luminous at the points where it attaches to the rails and these attachment points are visible in the 0.1 ms top-down view. The luminosity from the main body of the arc is cut-off due to the camera neutral-density filter. At 0.32 ms and 0.754 ms the intensity and luminosity from the arc has grown significantly, such that the entire arc column is observed in the image. The arc current at these times are about 1.75 kA and 3.2 kA, respectively. The frontal view at these times indicates the spatial extent of the arc in the spanwise and perpendicular directions to the surface. The arc is observed to have a dimension exceeding 1 cm in the spanwise direction and has about the same dimension in the perpendicular direction. The potential flow actuation area for the device is therefore significantly greater than a DBD actuator where the non-equilibrium streamer/corona plasma that is responsible for electrostatic flow actuation has a dimension of less than 1 mm [7]. In the last image at 2.24 ms, the arc has nearly extinguished as it approaches the end of the rail.

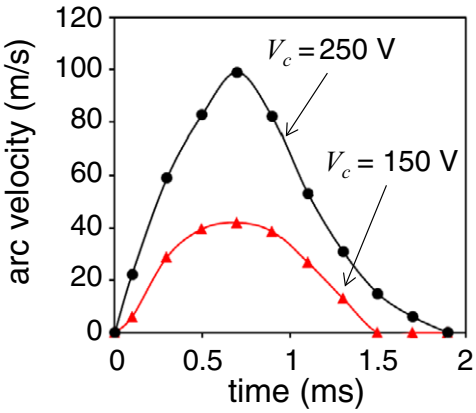


**Figure 8.** Plasma arc velocity as a function of time and capacitor voltage.

The high-speed imaging video also revealed other important features of the discharge structure. The arc was observed to attach to the rail electrode surface through one or more arc spots at any given time instance. These arc spot attachment points result from filament-like branching of the main arc column in the vicinity of the electrodes. Individual arc spots were observed to remain at fixed positions on the rail surface. The arc motion itself was facilitated by the formation of a new spot(s) ahead of the original spot in the direction of the propagation of the arc. As the arc column moves, the original spot is extinguished and the process repeats throughout the discharge transient. Note that the fluctuations in the voltage transient seen in figure 5 may be attributed to this arc spot formation-destruction process. Despite the filamentation of the arc in the vicinity of the electrode attachment points, the arc column itself remains intact during the transient and therefore the flow forcing due to bulk motion of the arc column is sustained.

Figure 8 shows the arc velocity for the two initial capacitor voltages discussed in figure 5. The arc velocity increases rapidly after initiation and reaches maximum values of about 40 m s$^{-1}$ for $V_c = 150$ V and 120 m s$^{-1}$ for $V_c = 250$ V around 0.7 ms into the transient. Following this maximum, the velocity decreases to zero. The arc velocity transient, including the time of peak velocity coincides with the arc current transient. Figure 9 displays the efficiency of the pulse forming network as a function of plasma arc peak velocity and $V_c$. At higher values of $V_c$, the plasma arc achieves a higher peak velocity. For both $V_c$ of 150 V and 250 V the RailPAc uses about 48% of the available capacitor bank energy to drive the plasma arc.

The transient velocity measured by the LDA was synchronously averaged using the capacitor voltage signal as a trigger. Figure 10 shows the LDA signal (seed particle velocity) and the capacitor voltage signal with respect to a

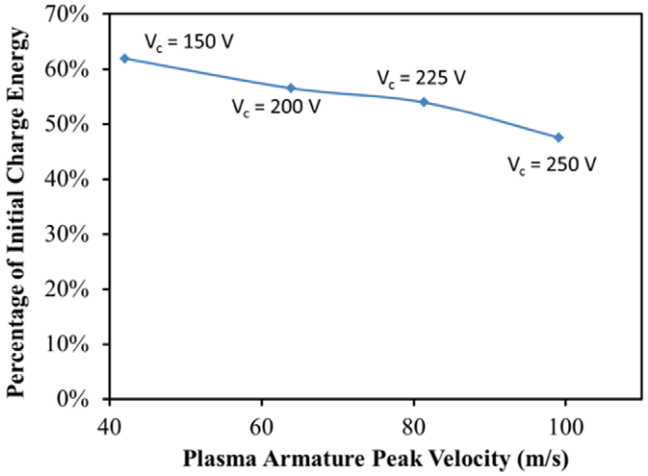


**Figure 9.** Ratio of plasma arc energy to initial capacitor bank energy as a function of plasma arc peak velocity.

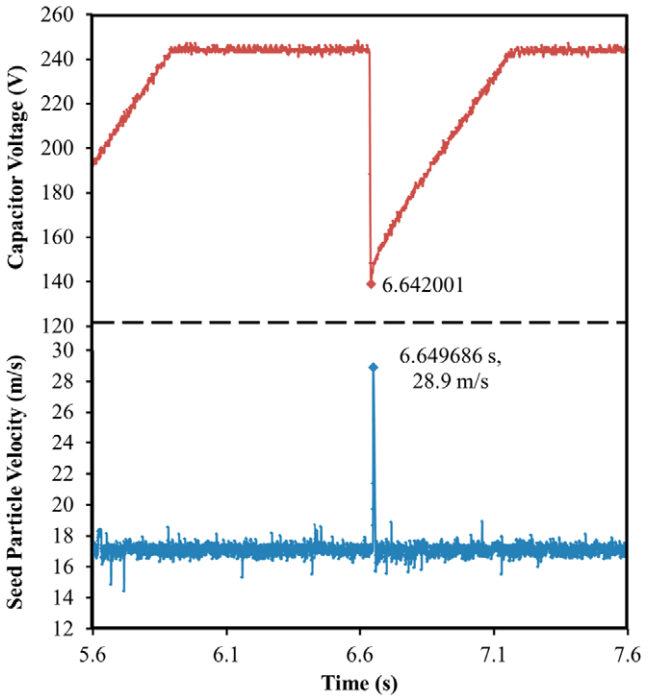


**Figure 10.** Capacitor voltage used as a trigger signal and LDA output signal showing seed particle velocity.

common time reference. This velocity was measured at the 225 mm $x$-location and about 5 mm above the airfoil surface. Therefore, although the freestream velocity of the wind tunnel is approximately 16 m s$^{-1}$, the mean velocity at this location is around 17 m s$^{-1}$ due to local airfoil curvature. The sudden drop in voltage indicates the initiation of the plasma arc at the breech. The large spike in the LDA signal at 6.6 s is the result of the induced flow wall jet passing through the focal point of the LDA. It is seen that at about 7.7 ms after the initiation of plasma arc there is an increase in the flow velocity from the mean of 17 m s$^{-1}$ to 29 m s$^{-1}$. The pulse forming network is designed to drive the plasma from the breech, located 37 mm aft of the leading edge (10% chord), along the rails to 223 mm aft of the leading edge (60% chord).

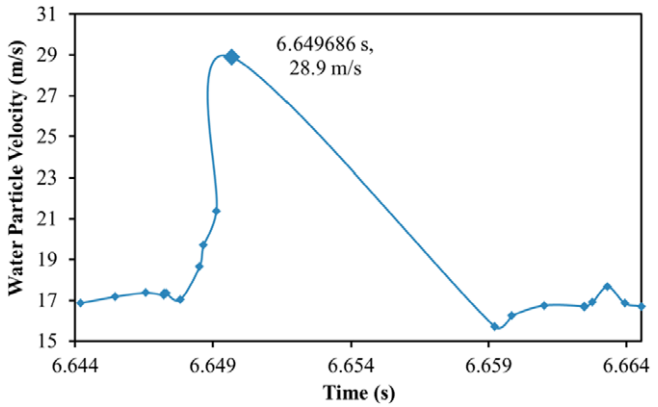


**Figure 11.** Transient increase in seed particle velocity due to plasma arc motion.

The LDA spatial focal point was 2 mm aft of the plasma arc termination point. Given the time to transit the rails of 2.25 ms and the delay due to the entrainment effects, the induced flow created by the plasma arc on the neutral air reaches a maximum velocity at approximately 8 ms after plasma arc initiation, at this particular spatial location. In general, it was observed that peak velocities occurred every 2–9 ms after plasma arc discharge depending on the measurement location.

Figure 11 shows a zoomed in view of the velocity spike at about 6.6 ms. A rapid increase of seed particle velocity is evident, followed by an absence of seed particles for around 10 ms. This is due to the plasma arc pushing seed particles away from the measurement volume as it travels downstream. Therefore, multiple such transient signals are required to reconstruct the induced velocity with sufficient confidence. Voids in the measured velocity due to random arrival and motion of seed particles is an inherent limitation of the LDA technique.

At a given chordwise location, the peak induced velocity as a function of height from the airfoil surface yields the velocity profile of the induced flow. Figure 12 shows the velocity profile of the induced flow created by the RailPAc compared to the velocity profile of the flow over the passive airfoil. The RailPAc is observed to induce a wall jet with a peak induced velocity of about 16 m s$^{-1}$ above the free stream velocity. The location of the peak velocity is at 7.5 mm above the airfoil surface and the effect of the RailPAc induced velocity is evident up to 45 mm above the surface. These induced flow velocities are significantly higher than those obtained with DBD actuators and can further be increased with careful optimization of the rail geometry, pulse energy and pulse duration. Also, the RailPAc induces flow over a large volume of air, over a height significantly greater than the boundary layer thickness.

## 5. Conclusions

In summary, we have described a magnetohydrodynamic plasma actuator for aerodynamic flow control. The actuator comprises a pair of rail electrodes over which a pulsed, low-voltage, high-current arc propagates to produce an induced

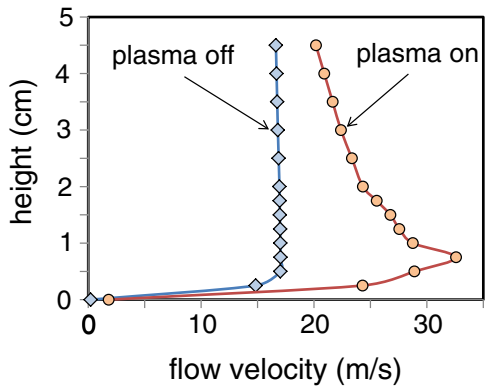


**Figure 12.** Comparison of velocity profiles over the airfoil at 60% chord with an incident velocity of 16 m s$^{-1}$. Solid diamonds indicate mean velocity profile of passive airfoil. Solid circles indicate peak velocity induced by RailPAc.

air wall jet. The arc motion is sustained by a self-induced magnetic field in the current loop formed by the rails and the arc, without need for external magnetic fields. Arc velocities of ∼10's m s$^{-1}$ are achieved for deposited pulse energies of ∼100 J in a stagnant air environment. The arc dimension in the direction perpendicular to the surface is of order 1 cm, resulting in significant penetration of the flow actuation effect away from the surface. The induced flow velocity measurements were performed with the rail plasma actuator mounted chordwise on an airfoil that was placed at zero angle of attack in a low-speed open test section wind tunnel. The air free stream velocity in the test section was 16 m s$^{-1}$. Results demonstrate the formation of a strong wall jet induced by the rail plasma actuator with peak induced velocities of about 16 m s$^{-1}$ for the specific conditions of our experiments. These induced velocities are significantly higher than those achievable with dielectric barrier discharge flow actuators.

## Acknowledgment

This work is supported by the US Army Research Office under a Short Term Innovative Research (STIR) award with Dr Frederick Ferguson as Program Monitor.

## References

[1] Cattafesta L N and Sheplak M 2011 *Annu. Rev. Fluid Mech.* **43** 247
[2] Post M L and Corke T C 2004 *AIAA J.* **42** 2177
[3] Santhanakrishnan A and Jacob J D 2007 *J. Phys. D: Appl. Phys.* **40** 637
[4] Patel M P, Ng T T, Vasudevan S, Corke T C and He C 2007 *J. Aircraft* **44** 1264
[5] Jolibois J and Moreau E 2009 *IEEE Trans. Dielectr. Electr. Insul.* **16** 758
[6] Corke T C, Enloe C L and Wilkinson S P 2010 *Annu. Rev. Fluid Mech.* **42** 505
[7] Likhanskii A V, Shneider M N, Macheret S O and Miles R B 2007 *Phys. Plasmas* **14** 073501
[8] Opaits D F, Likhanskii A V, Neretti G, Zaidi S, Shneider M N, Miles R B and Macheret S O 2008 *J. Appl. Phys.* **104** 043304
[9] Post M L and Corke T C 2006 *AIAA J.* **44** 3125
[10] Shin J, Narayanaswamy V, Raja L L and Clemens N T 2007 *AIAA J.* **45** 1596
[11] Samimy M, Adamovich I V, Webb B, Kastner J, Hileman J, Keshav S and Palm P 2004 *Exp. Fluids* **37** 577
[12] Narayanaswamy V, Raja L L and Clemens N T 2010 *AIAA J.* **48** 297
[13] Bose T K 1972 *AIAA J.* **10** 80
[14] Kelkar M and Heberlein J 2000 *J. Phys. D: Appl. Phys.* **33** 2172
[15] Kalra C H, Zaidi S, Miles R B and Macheret S O 2011 *Exp. Fluids* **50** 547
[16] Tropea C, Yarin A and Foss J (ed) 2007 *Springer Handbook of Experimental Fluid Mechanics* (Berlin: Springer) pp 215–471 chapter 5